LETTER

doi:10.1038/nature20787

Hydroclimate changes across the Amazon lowlands over the past 45,000 years

Xianfeng Wang[1,2], R. Lawrence Edwards[3], Augusto S. Auler[4], Hai Cheng[3,5], Xinggong Kong[6], Yongjin Wang[6], Francisco W. Cruz[7], Jeffrey A. Dorale[8] & Hong-Wei Chiang[1]

Reconstructing the history of tropical hydroclimates has been difficult, particularly for the Amazon basin—one of Earth's major centres of deep atmospheric convection[1,2]. For example, whether the Amazon basin was substantially drier[3,4] or remained wet[1,5] during glacial times has been controversial, largely because most study sites have been located on the periphery of the basin, and because interpretations can be complicated by sediment preservation, uncertainties in chronology, and topographical setting[6]. Here we show that rainfall in the basin responds closely to changes in glacial boundary conditions in terms of temperature and atmospheric concentrations of carbon dioxide[7]. Our results are based on a decadally resolved, uranium/thorium-dated, oxygen isotopic record for much of the past 45,000 years, obtained using speleothems from Paraíso Cave in eastern Amazonia; we interpret the record as being broadly related to precipitation. Relative to modern levels, precipitation in the region was about 58% during the Last Glacial Maximum (around 21,000 years ago) and 142% during the mid-Holocene epoch (about 6,000 years ago). We find that, as compared with cave records from the western edge of the lowlands, the Amazon was widely drier during the last glacial period, with much less recycling of water and probably reduced plant transpiration, although the rainforest persisted throughout this time.

Paraíso Cave (4° 4′ S, 55° 27′ W; 60 metres above sea level (a.s.l.)) is located near the centre of the eastern Amazon lowlands, which are densely covered by rainforest (see Methods and Extended Data Fig. 1a, b). The local climate is strongly influenced by prevailing easterly winds, which transport moisture year round from the tropical Atlantic Ocean to the basin (Extended Data Fig. 2a, b). The mean annual temperature at the site is about 26 °C, with a small seasonal fluctuation of around 2 °C. The annual precipitation exceeds 2,400 mm, with nearly 70% of this falling during the wet season (November to June; Extended Data Fig. 2c).

Our results are based on high-resolution speleothem oxygen-isotope analysis of seven calcite specimens, which were broken and columnar in shape when collected from Paraíso Cave (see Methods, Extended Data Fig. 3a, b, and Supplementary Information). We determined the chronologies of the specimens using a recently improved uranium/thorium dating technique (see Methods). Thanks to high uranium concentrations (up to 40 parts per million, p.p.m.) but low thorium concentrations (as low as 10 parts per trillion, p.p.t.), the ages of the samples are well constrained. The record is made up of 106 uranium/thorium dates, and 2,196 oxygen and carbon stable-isotope analyses, and has a temporal resolution in terms of stable isotope measurements of 5–30 years (Fig. 1).

The Paraíso Cave record spans the past 45 thousand years (kyr), with the exception of three short gaps (see Methods). We found that Paraíso $\delta^{18}O$ levels (where $\delta^{18}O = [(^{18}O/^{16}O)_{sample}/(^{18}O/^{16}O)_{standard} - 1] \times 1{,}000‰$) shifted between −3.0‰ and −5.0‰ on millennial timescales from 25 kyr to 45 kyr BP (before present, where 'present' means AD1950) in marine isotope stage 3 (MIS 3). After this interval, $\delta^{18}O$ increased, reaching values as high as −2.3‰ between 19 kyr and 21 kyr BP, during the Last Glacial Maximum (LGM). The oxygen isotopic ratio broadly decreased throughout the last deglaciation, reaching about −4.0‰ between 14.9 kyr and 16.8 kyr BP (at about the time of Heinrich stadial 1, HS1). $\delta^{18}O$ continued to decrease and reached values of −6.0‰ in the early Holocene, and then a minimum of about −8.7‰ during the mid-Holocene, between 5 kyr and 6 kyr BP, before increasing to the modern value of −6.0‰. The two most remarkable aspects of the Paraíso record are the large, dramatic shift in $\delta^{18}O$ values from the glacial period to the Holocene—a shift of 6.4‰—and the millennial-scale features in the glacial period (Fig. 1).

The replicating $\delta^{18}O$ profiles of contemporaneous growth intervals of different stalagmites, together with other lines of evidence (see Methods and Extended Data Figs 4a, b and 5a, b), demonstrate that the $\delta^{18}O$ change is dominated by a climate signal, rather than being disturbed by water–rock interactions or by kinetic fractionation. As it is unlikely that cave temperatures have changed by more than 5–6 °C over the past 45 kyr in the tropical lowlands[8,9], we infer that most of the $\delta^{18}O$ variability in our record results from changes in precipitation $\delta^{18}O$.

The eastern Amazon underlies an enormous atmospheric deep convection zone, a landward extension of the intertropical convergence zone (ITCZ). Because of its proximity to the tropical Atlantic Ocean, moisture entering this region has undergone only minor water recycling along air-transport routes[10]; changes in rainfall $\delta^{18}O$ therefore largely reflect a Rayleigh fractionation process, by which water vapour enriched in ^{18}O is progressively removed from air masses. Indeed, meteorological observations and model simulations show that variation in regional rainfall $\delta^{18}O$ is predominantly controlled by precipitation amount[11–13]. If so, Paraíso $\delta^{18}O$ is negatively correlated with rainfall, and is largely determined by moist convection in the eastern Amazon.

The large shift in $\delta^{18}O$ values in the Paraíso record indicates a substantial increase in convection intensity and rainfall over the eastern basin from glacial times to the Holocene. Considering that the tropical Atlantic is the single dominant moisture source, we can use the Rayleigh distillation model[11] as an approximation to calculate the fraction of water vapour lost from air masses between the tropical Atlantic and the eastern Amazon (see Methods and Extended Data Fig. 1b). A similar calculation is valid for glacial times as well, because the continental shelf off the Amazon River mouth was not widely exposed even during the LGM[2]. We assume that, relative to the pre-industrial present, the Amazon basin endured a cooling of about 5 °C in the LGM[8], but a subtle warming of about 0.5 °C in the mid-Holocene[14] (see Methods). The percentage of water vapour lost before reaching Paraíso is then about 28%, 50% and 36% during the LGM, mid-Holocene and today, respectively (Methods and Extended Data Table 1). As the relative

[1]Earth Observatory of Singapore, Nanyang Technological University, 639798 Singapore. [2]Asian School of the Environment, Nanyang Technological University, 639798 Singapore. [3]Department of Earth Sciences, University of Minnesota, Minneapolis, Minnesota 55455, USA. [4]Instituto do Carste, Belo Horizonte, Minas Gerais 30150-160, Brazil. [5]Institute of Global Environmental Change, Xi'an Jiaotong University, Xi'an 710049, China. [6]School of Geography Science, Nanjing Normal University, Nanjing 210023, China. [7]Instituto de Geociências, Universidade de São Paulo, São Paulo 05508-080, Brazil. [8]Department of Earth & Environmental Sciences, University of Iowa, Iowa City, Iowa 52242, USA.

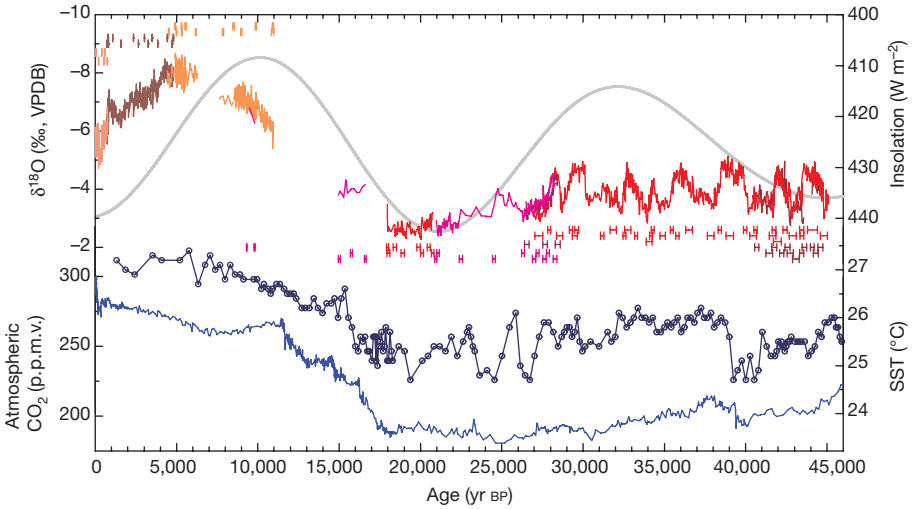

Figure 1 | Paraíso speleothem record, and comparisons with local summer insolation, tropical Atlantic SST and atmospheric CO_2 concentration. Top, the Paraíso record is spliced by replicated $\delta^{18}O$ profiles from seven stalagmite samples. Uranium/thorium dates and error bars (2σ) are shown, with different colours for each stalagmite sample. The record covers the past 45,000 years, with three short gaps: ~16.6 kyr to 18.0 kyr BP, ~10.9 kyr to 15.0 kyr BP, and ~6.3 kyr to 7.6 kyr BP. The insolation at 5° S in January is also shown, in grey; note that the insolation is plotted in a reversed scale, as proposed in ref. 16. The correlation between the Paraíso $\delta^{18}O$ values and local insolation is, however, not strong. See Extended Data Fig. 6 for more details. Centre, tropical Atlantic alkenone SST reconstruction from sediment core GeoB 3910-2 (in dark blue, ref. 19). Bottom, changes in atmospheric CO_2 concentration[7] (in light blue; see also Extended Data Fig. 7). p.p.m.v., parts per million by volume.

humidity has probably remained close to 100% in the deep basin, then the precipitation amount integrated from source to the cave site was about 142% and 58% of today's during the mid-Holocene and LGM, respectively.

What may have caused such large changes in precipitation in the eastern Amazon? Local summer insolation is often suggested as the major factor that is forcing hydroclimate change in the region[1,15–17]. The overall Paraíso record, however, does not obviously follow local insolation change, although it does cover two precessional cycles (Fig. 1 and Extended Data Fig. 6). The largest shift in Paraíso $\delta^{18}O$ occurred during the last deglaciation—the time interval that saw an increase in the atmospheric CO_2 concentration of about one-third[7] (Fig. 1, Extended Data Fig. 7). Proxy data and climate model simulations have indicated a pivotal role of CO_2 in driving the deglacial warming[18]. Therefore, the reduced influence of insolation in our record probably implies that, at least in the eastern Amazon lowlands, regional convection is controlled largely by temperature changes associated with atmospheric CO_2 levels. During the LGM, a drop in sea surface temperature (SST) of about 2–3 °C in the equatorial western Atlantic[19], accompanied by a cooling of around 5 °C on land[8], could have suppressed moisture supply from the ocean and reduced convection in the basin[20]. In contrast, warming in the mid-Holocene probably enhanced the upward motion of moisture and resulted in more abundant precipitation. However, the $\delta^{18}O$ increase of about 2.3‰ through the past 5,000 years may not solely be attributed to a temperature change that was rather subtle[14]. Under modern climatic conditions, periodic Amazon droughts—particularly in the eastern and central regions—are closely tied to positive SST anomalies in the eastern tropical Pacific[21]. Thus, a strengthening of El Niño/Southern Oscillation (ENSO) activity[22] could have exacerbated rainfall decrease and water $\delta^{18}O$ increase after the mid-Holocene. Alternatively, under interglacial boundary conditions, it is possible that local insolation[1,15–17] contributed to the observed Holocene changes.

During MIS 3, the Paraíso record shows strong millennial-scale variability, as a manifestation of Heinrich and Dansgaard–Oeschger (D/O) climate events. These variations coincide with, but in an anti-phased fashion, their counterparts observed in eastern China[23,24], and can also be correlated one-to-one with the rapid events in Greenland and Antarctica[25] (Fig. 2 and Extended Data Fig. 8a, b). The latitudinal displacement of the mean position of the ITCZ, in response to changes in the Atlantic meridional ocean circulation (AMOC), may well have caused the anti-phased abrupt change in rainfall between the two low-latitude regions[15]. Perturbations in the AMOC can induce SST anomalies in the tropical oceans—anomalies that then alter moist convections and rainfall in the region. In this regard, the remarkably tight correlations among these records reinforce the notion that abrupt changes occurring in high latitudes can be rapidly propagated in the climate system, probably through an atmospheric linkage[15].

Were the aforementioned large glacial-to-Holocene rainfall changes mainly confined to the eastern Amazon, or were they more extensive in the lowlands? Existing records from the Amazon basin and its surrounding areas draw a contentious picture of rainfall changes during the LGM and the last deglaciation, compromised by less-than-ideal chronological control, sediment preservation and topographic effects (see, for example, refs 1–6). Meanwhile, several studies suggest a strong South American summer monsoon (SASM) intensity during the LGM, and hence higher rainfall in the central Andes and southern Brazil[1,15,16]. But these sites are not located within the basin itself.

We here compare the Paraíso record with speleothem $\delta^{18}O$ profiles obtained from caves in the western lowlands near the eastern flank of the Andes (5° 44′ S, 77° 30′ W; ~960 m a.s.l.; Extended Data Fig. 1a, b)[9,17], to assess surface moisture transport across the basin and spatial changes in precipitation (Fig. 3). During MIS 3, there is a substantial $\delta^{18}O$ offset of about 4.5‰ to 5.1‰ between the Paraíso record from the eastern Amazon and the temperature-effect-corrected Diamante/Tigre Perdido record from the western Amazon (Methods). While the oxygen isotope ratio in the Paraíso samples is higher, varying between −3.0‰ and −5.0‰, $\delta^{18}O$ values are about −8.1 to −9.5‰ in the Diamante profile (after correction for isotopic fractionation caused by cave temperature differences). This east-to-west difference is further enhanced during the LGM, by up to 6.6‰. However, the two records show similar values during the early to mid-Holocene, and their values differ by only about 2.5‰ at present.

The change in $\delta^{18}O$ offset between the two records, which essentially describes a change in the gradient of rainfall $\delta^{18}O$ across the basin, signifies a shift in the dominant isotope-fractionation process over time. Lower $\delta^{18}O$ values in the western Amazon samples relative to those in Paraíso are consistent with the overall continental rainout

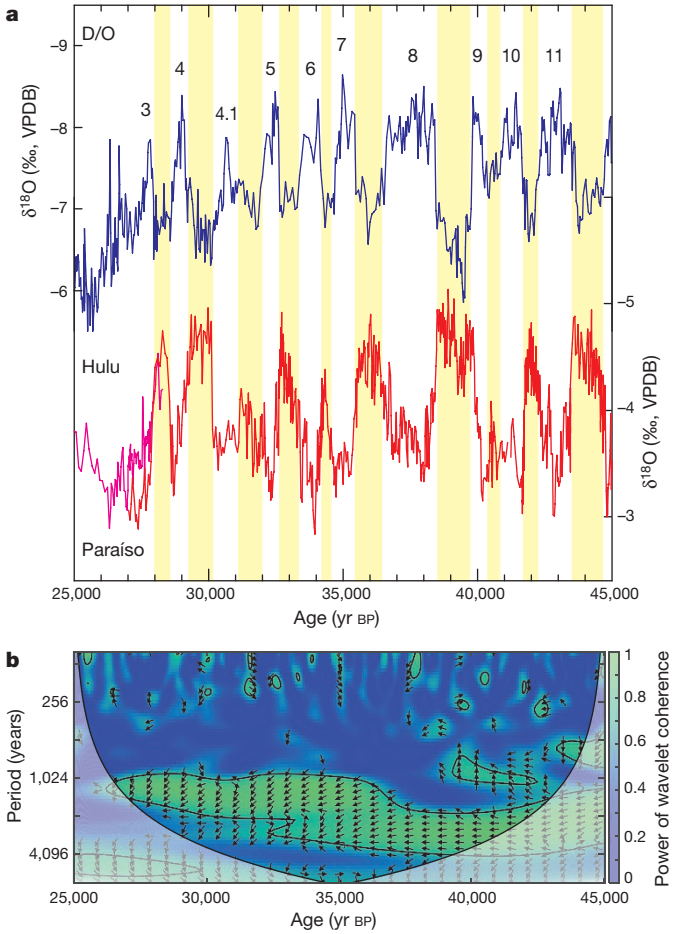

Figure 2 | Comparisons of eastern Amazon and eastern China stalagmite records. a, Stalagmite $\delta^{18}O$ records from the eastern Amazon (Paraíso, in red and pink) and eastern China (Hulu, in blue)[24] for the time interval from 25 kyr BP to 45 kyr BP. These records are oppositely correlated on millennial timescales, suggesting an anti-phased relationship for rainfall between the two regions. D/O climate events (numbered from 3 to 11) are also marked. **b**, The strong anti-phased correlation between the two records on millennial timescales is confirmed by squared wavelet coherence (http://noc.ac.uk/using-science/crosswavelet-wavelet-coherence) of the two standardized time series. The 5% significance level against red noise is shown as a thick contour. The relative phase relationship between the two time series is shown as arrows, with anti-phase pointing left.

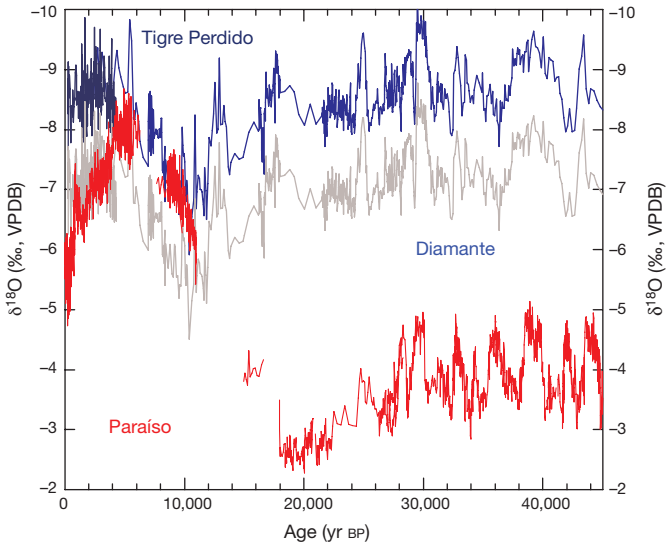

Figure 3 | Comparisons of speleotherm records from the eastern and western Amazon. The eastern Amazon $\delta^{18}O$ record (red) is from Paraíso cave; the speleothem $\delta^{18}O$ records in the western Amazon are from Diamante[17] (blue) and Tigre Perdido[9] (dark blue; left) caves. All three records are absolutely dated with uranium/thorium dating techniques. The original records from the western Amazon are shown in grey; they were then shifted 1.4‰ negatively to account for the oxygen isotopic fractionation that resulted from a difference in cave temperature between the western sites and Paraíso cave in the east (see Methods).

effect of water isotopes[11] when surface moisture is transported from the east to the west across the lowlands. Indeed, given the vast distance between the two locations (around 2,400 km), the spatial rate of speleothem $\delta^{18}O$ change is −1.0‰ per 1,000 km, in concert with the precipitation $\delta^{18}O$ gradient observed today in the lowlands, being −0.1‰ per degree longitude[12]. This gradient is, however, very low, largely because of water recycling in the basin, through plant transpiration in particular. Plant transpiration supplies moisture downwind, yet does not induce water isotope fractionation when the ambient humidity is high in the tropics[26,27]. Such an effect—probably resulting from the much denser rainforest coverage in the basin—almost completely dominates during the early to mid-Holocene, as shown in the nearly identical $\delta^{18}O$ values of the two speleothem records. In contrast, the precipitation $\delta^{18}O$ gradient reached as high as −2.8‰ per 1,000 km during the LGM. This strongly suggests that, during glacial times, the Amazon basin was much drier with reduced rainforest coverage, in accordance with studies of marine and lacustrine sediments[2,4]. Therefore, the continental effect dictated the isotopic fractionation and led to a progressive depletion in ^{18}O in rainfall when moisture was transported across the basin, whereas the effect of plant transpiration was much less.

As the largest tropical wetland, the Amazon basin is, in warm, wet times, a substantial contributor to global methane production through enhanced microorganism activity; conversely, a cold, dry Amazon basin during the LGM probably contributed to the drop in atmospheric methane that is recorded in ice cores from this time (Extended Data Fig. 7). This might explain the controversy that Asian monsoon intensity was relatively strong during the LGM, while atmospheric methane abundance declined to its lowest value[7,23]. During MIS 3, however, there is a positive correlation between methane concentration and Paraíso $\delta^{18}O$ on millennial timescales, which confirms that Northern Hemisphere tropical and boreal wetlands have been the dominant sources of methane[7,24]. In contrast to a dry Amazon during the LGM, the values of $\delta^{13}C$ in Paraíso stalagmites can be as low as −10‰, comparable with those in Holocene samples (Extended Data Fig. 9). This indicates that the Amazon basin was not dry enough during the LGM or at any time within the past 45 kyr for the forest to have turned into a savanna with substantial C4 vegetation. Rainforest has persisted in the eastern Amazon even when rainfall amounts were only about 60% of today's values during the LGM.

If our observed pattern of Amazonian hydroclimate change from the last glacial period to the Holocene can be extrapolated to a CO_2-induced warming future, rainfall in the Amazon lowlands could be expected to increase substantially, being consistent with the 'wet wetter, dry drier' mechanism[28]. Ironically, however, ongoing deforestation and expansion of plantations in the basin, particularly in the eastern region, as well as a possible intensification of ENSO[21,29] may reduce water recycling through plant transpiration; therefore, this would reduce moisture delivery to the west[30]. Whether or not the long-lasting Amazon rainforest can be sustained in the future remains an open question.

Online Content Methods, along with any additional Extended Data display items and Source Data, are available in the online version of the paper; references unique to these sections appear only in the online paper.

Received 18 July; accepted 8 November 2016.

1. Baker, P. A. *et al.* The history of South American tropical precipitation for the past 25,000 years. *Science* **291,** 640–643 (2001).
2. Maslin, M. A. *et al.* Dynamic boundary-monsoon intensity hypothesis: evidence from the deglacial Amazon River discharge record. *Quat. Sci. Rev.* **30,** 3823–3833 (2011).
3. Ledru, M.-P., Bertaux, J. & Sifeddine, A. Absence of Last Glacial Maximum records in lowland tropical forests. *Quat. Res.* **49,** 233–237 (1998).
4. D'Apolito, C., Absy, M. L. & Latrubesse, E. M. The Hill of Six Lakes revisited: new data and re-evaluation of a key Pleistocene Amazon site. *Quat. Sci. Rev.* **76,** 140–155 (2013).
5. Colinvaux, P. A. *et al.* A long pollen record from lowland Amazonia: forest and cooling in glacial times. *Science* **274,** 85–88 (1996).
6. Baker, P. A. & Fritz, S. C. Nature and causes of Quaternary climate variation of tropical South America. *Quat. Sci. Rev.* **124,** 31–47 (2015).
7. Marcott, S. A. *et al.* Centennial-scale changes in the global carbon cycle during the last deglaciation. *Nature* **514,** 616–619 (2014).
8. Stute, M. *et al.* Cooling of tropical Brazil (5°C) during the Last Glacial Maximum. *Science* **269,** 379–383 (1995).
9. van Breukelen, M. R. *et al.* Fossil dripwater in stalagmites reveals Holocene temperature and rainfall variation in Amazonia. *Earth Planet. Sci. Lett.* **275,** 54–60 (2008).
10. Eltahir, E. A. B. & Bras, R. L. Precipitation recycling in the Amazon Basin. *Q. J. R. Meteorol. Soc.* **120,** 861–880 (1994).
11. Dansgaard, W. Stable isotopes in precipitation. *Tellus* **16,** 436–468 (1964).
12. Vuille, M. *et al.* Modeling $\delta^{18}O$ in precipitation over the tropical Americas: 1. Interannual variability and climatic controls. *J. Geophys. Res.* **108** (D6), 4174 (2003).
13. Lee, J.-E., Johnson, K. & Fung, I. Precipitation over South America during the Last Glacial Maximum: an analysis of the "amount effect" with a water isotope-enabled general circulation model. *Geophys. Res. Lett.* **36,** L19701 (2009).
14. Wanner, H. *et al.* Mid- to late Holocene climate change: an overview. *Quat. Sci. Rev.* **27,** 1791–1828 (2008).
15. Wang, X. *et al.* Millennial-scale precipitation changes in southern Brazil over the past 90,000 years. *Geophys. Res. Lett.* **34,** L23701 (2007).
16. Cruz, F. W. *et al.* Orbitally driven east-west antiphasing of South American precipitation. *Nat. Geosci.* **2,** 210–214 (2009).
17. Cheng, H. *et al.* Climate change patterns in Amazonia and biodiversity. *Nat. Commun.* **4,** 1411 (2013).
18. Shakun, J. D. *et al.* Global warming preceded by increasing carbon dioxide concentrations during the last deglaciation. *Nature* **484,** 49–54 (2012).
19. Jaeschke, A., Rühlemann, C., Arz, H., Heil, G. & Lohmann, G. Coupling of millennial-scale changes in sea surface temperature and precipitation off northeastern Brazil with high-latitude climate shifts during the last glacial period. *Paleoceanography* **22,** PA4206 (2007).
20. Cook, K. H. & Vizy, E. K. South American climate during the Last Glacial Maximum: delayed onset of the South American monson. *J. Geophys. Res.* **111,** D02110 (2006).
21. Malhi, Y. *et al.* Climate change, deforestation, and the fate of the Amazon. *Science* **319,** 169–172 (2008).
22. Koutavas, A. & Joanides, St. El Niño-Southern Oscillation extrema in the Holocene and Last Glacial Maximum. *Paleoceanography* **27,** PA4208 (2012).
23. Wang, Y. J. *et al.* A high-resolution absolute-dated Late Pleistocene monsoon record from Hulu Cave, China. *Science* **294,** 2345–2348 (2001).
24. Cheng, H. *et al.* The Asian monsoon over the past 640,000 years and ice age terminations. *Nature* **534,** 640–646 (2016).
25. WAIS Divide Project Members. Precise interpolar phasing of abrupt climate change during the last ice age. *Nature* **520,** 661–665 (2015).
26. Salati, E., Dall'Olio, A., Matsui, E. & Gat, J. R. Recycling of water in the Amazon Basin: an isotopic study. *Wat. Resour. Res.* **15,** 1250–1258 (1979).
27. Winnick, M. J., Chamberlain, C. P., Caves, J. K. & Welker, J. M. Quantifying the isotopic 'continental effect'. *Earth Planet. Sci. Lett.* **406,** 123–133 (2014).
28. Held, I. M. & Soden, B. J. Robust response of the hydrological cycle to global warming. *J. Clim.* **19,** 5686–5699 (2006).
29. Vecchi, G. A. *et al.* Weakening of tropical Pacific atmospheric circulation due to anthropogenic forcing. *Nature* **441,** 73–76 (2006).
30. Spracklen, D. V., Arnold, S. R. & Taylor, C. M. Observations of increased tropical rainfall preceded by air passes over forests. *Nature* **489,** 282–285 (2012).

Supplementary Information is available in the online version of the paper.

Acknowledgements This work was supported by a Singapore National Research Foundation (NRF) Fellowship (NRFF2011-08) and a Gary Comer Fellowship to X.W.; US National Science Foundation (NSF) grants 1103404 and 1317693 to R.L.E. and H.C.; a Brazil National Council for Scientific and Technological Development (CNPq) grant (540064/01-7) to A.S.A.; grants from the China National Basic Research Program (NBRP; 2013CB955902) and the National Natural Science Foundation of China (NSFC; 41230524) to H.C.; and a grant from the São Paulo Research Foundation of Brazil and US NSF Dimensions of Biodiversity joint program (FAPESP/NSF; 2012/50260-6) to F.W.C. Field travelling funds were partially supported by a National Geographical Society grant, 7574-03. We acknowledge the help of colleagues from the Grupo Bambuí de Pesquisas Espeleológicas with cave mapping and sampling. We thank R. Fonseca, S. Yuan, Y. Lu and Y. Djamil for assistance with the figures concerning wind fields and regional rainfall, and B. Wohlfarth and S. Hemming for discussions during manuscript preparation.

Author Contributions X.W., R.L.E. and A.S.A. designed the project. X.W., A.S.A. and J.A.D. performed the fieldwork and sampling. X.W. and H.-W. C. carried out the uranium/thorium dating. X.W., X.K. and Y.W. contributed to the oxygen-isotope measurements. X.W. wrote the manuscript, which was edited by R.L.E. and other authors. All authors discussed the results and implications and commented on the manuscript at all stages.

Author Information Reprints and permissions information is available at www.nature.com/reprints. The authors declare no competing financial interests. Readers are welcome to comment on the online version of the paper. Correspondence and requests for materials should be addressed to X.W. (xianfeng.wang@ntu.edu.sg).

Reviewer Information *Nature* thanks M. Bush, J. Shakun and the other anonymous reviewer(s) for their contribution to the peer review of this work.

METHODS

Cave location and samples. Paraíso Cave (04° 04′ S, 55° 27′ W, 60 m a.s.l.) is located near the centre of the eastern Amazon lowlands, adjacent to the Tapajós River, which is one of the main tributaries of the Amazon River (Extended Data Fig. 1a, b). The cave is ~2.8 km long, overlaid by ~15-m-thick Pennsylvanian limestone of Itaituba Formation, and covered by dense tropical rainforest. The cave has a small single entrance. Gravels and boulders nearly block the initial chamber, which declines gradually towards an underground stream. The cave therefore has a very high relative humidity, near 100%.

We collected columnar stalagmites that were mostly broken, for reasons of ease of sampling and conservation. They were collected from scattered locations inside the cave. The stalagmites were cut into halves along their growth axes and their surfaces were polished. Seven of them were selected for this study. They are all composed of calcite, and some have clear banding structures.

Analytical methods. A total of 106 subsamples (16, 8, 13, 12, 41, 3 and 13 for stalagmites PAR01, PAR03, PAR16, PAR06, PAR07, PAR08 and PAR24, respectively) were drilled for uranium/thorium dating. Procedures for chemical separation and purification of uranium and thorium are similar to those described[31,32]. The dating analysis was performed at the Minnesota Isotope Laboratory, University of Minnesota, USA, on a ThermoFinnigan Neptune multi-collector inductively coupled plasma mass spectrometer (MC-ICP-MS), and also on a Neptune Plus instrument housed in a newly established isotope geochemistry laboratory at the Earth Observatory of Singapore, Nanyang Technological University. The measurements largely followed the methods described in refs 33, 34. All of the uranium and thorium isotopes, except ^{238}U and ^{232}Th, were measured with a peak-jumping mode on a secondary electron multiplier (SEM) equipped with a retarding potential quadrupole lens (RPQ) to improve abundance sensitivity. Consistent results were achieved with solution aliquots between the two laboratories.

All of the stalagmite samples have a high uranium concentration (a few parts per million) but a very low thorium concentration (typically around $n \times 10$ or $n \times 100$ parts per trillion) (Extended Data Fig. 3). The measured $^{230}Th/^{232}Th$ is in the range $n \times 1{,}000$ p.p.m. to $n \times 1{,}000{,}000$ p.p.m. in atomic ratio. We calculated corrected ^{230}Th ages using the bulk Earth initial $^{230}Th/^{232}Th$ value of 4.4 p.p.m. in atomic ratio, with an arbitrary uncertainty of 50%. Whatever the true initial $^{230}Th/^{232}Th$ value is, its contribution to the final uranium/thorium ages should be negligible. Uncertainties in the uranium/thorium isotopic data and ^{230}Th dates are then calculated at the 2σ level (two standard deviations of the mean). The typical relative error in age is less than 0.5%.

The uranium/thorium ages for all of the stalagmite samples are in stratigraphic order. The stalagmites have relatively fast and constant growth rates (Extended Data Fig. 3a, b). Their age models were hence established by linear interpolations.

Oxygen and carbon stable isotope analyses of stalagmite samples were carried out at the School of Geography Science, Nanjing Normal University, China. Calcite powder subsamples were milled with dental drill bits at intervals of 1–5 mm, and analysed on a Finnigan MAT 253 mass spectrometer equipped with a Kiel Carbonate Device III. Duplicate measurements of standard NBS19 and arbitrary samples show a long-term reproducibility of ~0.10‰ (1σ). In total, we carried out 2,196 oxygen and carbon isotopic measurements, comprising 449, 145, 406, 110, 820, 100 and 166 analyses from stalagmites PAR01, PAR03, PAR16, PAR06, PAR07, PAR08 and PAR24, respectively. This yields a temporal resolution about 5 to 30 years, slightly higher in the Holocene part than that during the last glacial period portion. Stable isotopic results are reported in per mil (‰), relative to the Vienna Pee Dee Belemnite (VPDB) standard: $(\delta^{18}O = [(^{18}O/^{16}O)_{sample}/(^{18}O/^{16}O)_{standard} - 1] \times 1{,}000‰)$.

Speleothems often have growth discontinuities owing to a wide range of factors, including changes in sea level, soil temperature or regional aridity, local cave flooding or drip-water dynamics[35]. Among the seven calcite specimens we used to construct the Paraíso Cave record, samples PAR06, PAR07, PAR16 and PAR24 present detectable growth hiatuses (Extended Data Fig. 3b). Nevertheless, the striking similarities between their $\delta^{18}O$ profiles of the seven samples over their contemporaneous growth periods strongly suggest that the dataset is robust. We hereby obtained a spliced record that spans the past 45,000 years, with three short gaps: ~16.6 kyr to 18.0 kyr BP, ~10.9 kyr to 15.0 kyr BP, and ~6.3 kyr to 7.6 kyr BP.

Equilibrium condition tests on carbonate deposition. Many processes other than climate—such as water–rock interactions in the vadose zone, and kinetic fractionation during carbonate precipitation—could contribute to the stable isotopic signal in speleothems. It is, however, very unlikely that the combination of hydrological processes experienced by water drips is identical, especially if we consider the different growth rates of different samples and the carbonate supersaturation state in water films[23,36].

The Paraíso $\delta^{18}O$ profiles present substantial replications between different samples, even when their growth rates are different by a factor of ten (compare, for example, PAR07 and PAR08; Extended Data Fig. 3b). Although no contemporaneous samples have been found yet during the LGM, PAR07 and PAR24 cover 19.0 kyr to 20.7 kyr BP, and 21.0 kyr to 22.8 kyr BP, respectively. Their $\delta^{18}O$ values during the LGM are essentially the same: $-2.72‰ \pm 0.23‰$ (1σ) and $-2.79‰ \pm 0.19‰$ (1σ), respectively. Therefore, the replication between the $\delta^{18}O$ profiles of contemporaneous samples strongly indicates that the Paraíso Cave speleothems were mostly deposited under equilibrium conditions, and that the influence of kinetic fractionation on the $\delta^{18}O$ record must be negligible.

In addition, the low correlation coefficients between the $\delta^{18}O$ and $\delta^{13}C$ values for most of the Paraíso Cave samples (Extended Data Fig. 4a, b) confirm that kinetic CO_2 degassing and water evaporation should have been minimal during calcite precipitation[37]. We further tested the equilibrium conditions in Paraíso Cave modern calcite depositions. The $\delta^{18}O$ values of about $-5.7‰$ found for modern calcite are a good approximation to the value of around $-5.8‰$ that is predicted under equilibrium conditions with a cave temperature of 26 °C and annual average rainfall $\delta^{18}O$ of about $-4.2‰$ (refs 38, 39). All of these lines of evidence suggest that calcite precipitation in Paraíso Cave mostly takes place under equilibrium conditions. Therefore, the $\delta^{18}O$ signal in the Paraíso Cave speleothems is dominated by climate variation at the time of calcite precipitation.

Calculations of moisture rainout in eastern Amazon. Paraíso Cave is in relative proximity to the coast. Moisture is brought into the region by the prevailing easterlies and has not endured strong water recycling along the air trajectory[10,40]. When water vapour is progressively removed from air masses during transport, the Rayleigh fractionation dictates, and results in a gradual depletion of ^{18}O in the remaining water vapour and subsequent precipitation[11]. We therefore, to first order, can use the standard Rayleigh distillation model to calculate what fraction of the moisture has been removed when it is integrated from the source region to the cave site (Extended Data Table 1). For the calculation, we adopt the equation: $(1{,}000 + \delta^{18}O_p)/(1{,}000 + \delta^{18}O_{sw}) = f^{(\alpha - 1)}$, where $\delta^{18}O_p$ and $\delta^{18}O_{sw}$ are the $\delta^{18}O$ signals of meteoric precipitation and seawater, respectively; f is the fraction of the original water vapour remaining in air masses; and α is the water/vapour fractionation factor.

The same calculation can be applied to moisture transport in the past, such as during the mid-Holocene and the LGM, because the exposure and submergence of the narrow continental shelf did not change dramatically the distance between the cave site and the moisture source[2]. Here, the time intervals of modern, mid-Holocene and LGM cover the past 1,000 years or so, the period from about 5,000 to 6,000 years BP, and the period from about 19,000 to 23,000 years BP, respectively, as defined in refs 14,41,42.

Relative to today's temperature of 26 °C, we assign cave temperatures of 26.5 °C and 21 °C during the mid-Holocene and LGM, respectively (Extended Data Table 1). This is after taking into consideration SST changes in the tropical Atlantic[14,19,42,43], as well as surface temperature changes reported from higher altitudes or from further inland[5,8,9]. The uncertainty in temperature estimation at the cave site is probably within 1 °C. To test the sensitivity of water vapour loss to temperature, we also applied different temperatures for the mid-Holocene (for example, the same as modern temperatures) and LGM (for example, 4 °C or 6 °C lower than today's value) (Extended Data Table 1b). The calculations show that the bulk estimations of water vapour loss are not sensitive to temperature change within the uncertainties of palaeotemperature reconstructions[5,8,14].

In the equatorial lowlands, it is reasonable to assume that the relative humidity is close to 100%, even when the surface temperature was ~5 °C lower during the LGM. We can thus further evaluate the absolute amount of moisture change through time (Extended Data Table 1).

The decrease in temperature and precipitation during the LGM could have affected the water balance in the region. At present, the mean annual rainfall is ~2,400 mm in the region—substantially higher than the annual evapotranspiration of ~1,200 mm (Extended Data Fig. 5a). If we assume that rainfall seasonality remained similar during the LGM in the wet tropics, then estimations of water balance[44,45] show that, through most of the months, precipitation could have remained higher than actual evapotranspiration (Extended Data Fig. 5b). Therefore, seasonal groundwater recharge did not change enough during the LGM to cause biases in the stable isotopic composition of Paraíso cave drip water.

East–west moisture isotope gradient. We can study changes in the moisture isotope gradient across the Amazon lowlands by comparing cave $\delta^{18}O$ records from nearly the longitudinal ends of the basin. For this study, we chose the speleothem records from Diamante Cave[17] and Cueva del Tigre Perdido[9], both located in the western lowland (5° 44′ S, 77° 30′ W, ~960 m a.s.l.), and compared them with the Paraíso record from the east. The Diamante record extends continuously through the time period discussed, and its uranium/thorium dates are better constrained relative to other cave records in the region. Cueva del Tigre Perdido is located near Diamante Cave, and shares the same elevation. Its $\delta^{18}O$ record has higher

resolution during the late Holocene, so we used this portion of the record for the spliced western profile.

In the tropics, below the height of the cloud base (at about 950 millibars), the air temperature drops as the altitude increases at a dry adiabatic lapse rate of $-9.7\,°C\,km^{-1}$ (ref. 46). Above the cloud base, the air temperature falls much more slowly, at a moist adiabatic lapse rate of $-5\,°C\,km^{-1}$ or less[47]. Nevertheless, because of the relatively low elevations of the caves, uncertainties in estimations of the lapse rate in a mountain region probably do not have a dramatic influence on the estimations of cave temperatures in the western Amazon, even between the glacial and interglacial periods[48]. However, the lapse rate can cause cave temperature differences between the east and west cave sites. Owing to the temperature dependence of calcite-water isotopic fractionation, these cave temperature differences will have contributed to the difference in the calcite $\delta^{18}O$ values of the two records. We here assign a constant, typical lapse rate of $6.5\,°C\,km^{-1}$, which leads to a temperature that is ~5.8 °C ($6.5\,°C\,km^{-1} \times 900\,m$) lower in the Diamante and Tigre Perdido caves than in Paraíso Cave. This number is consistent with the modern temperature difference between the caves (~26 °C and ~20 °C in Paraíso Cave and Cueva del Tigre Perdido, respectively)[9]. The temperature difference can transfer to an imprint of a ~1.4‰ calcite $\delta^{18}O$ increase ($-5.8\,°C \times (-0.24‰$ per °C)) in the Diamante/Tigre Perdido record. Such a temperature effect caused by a difference in elevation must be removed from the Diamante/Tigre Perdido record to facilitate comparison of the records. We therefore shifted the western profile about 1.4‰ more negatively relative to the original record (Fig. 3). In other words, the local rainfall $\delta^{18}O$ at the Amazon western sites should be lowered by ~1.4‰, assuming that carbonate deposition is under equilibrium conditions.

We calculated the offset between the two cave records by subtracting their contemporaneous $\delta^{18}O$ values. If speleothem calcite is deposited under equilibrium conditions, then such an offset is a good approximation to the discrepancy in rainfall $\delta^{18}O$ between the east and west cave sites after we remove the aforementioned temperature effect caused by their elevation difference. We can then obtain the precipitation $\delta^{18}O$ gradient across the Amazon basin by dividing the offset of speleothem $\delta^{18}O$ by the longitudinal distance (~2,400 km). Changes in cave temperature and ocean reservoir $\delta^{18}O$ related to sea-level fluctuations can contribute to each speleothem $\delta^{18}O$ signal, particularly on glacial–interglacial timescales. Such effects, however, are of the same magnitude in the two records, and therefore should be cancelled out in the offset. Indeed, through this method, we estimated a modern spatial rate of speleothem $\delta^{18}O$ change of ~1.0‰ per 1,000 km (~2.5‰ $\delta^{18}O$ offset divided by a distance of ~2,400 km). This is in agreement with the precipitation $\delta^{18}O$ gradient in the lowlands observed today (~0.1‰ per unit longitude)[12]. We therefore believe that, in the western Amazon, the effect of plant transpiration[26,27,49] is probably more important than the effect of rainfall amount in determining rainfall $\delta^{18}O$ and subsequent cave carbonate $\delta^{18}O$ values, broadly in line with the conclusions reached in ref. 17.

31. Edwards, R. L., Chen, J. H. & Wasserburg, G. J. ^{238}U-^{234}U-^{230}Th-^{232}Th systematics and the precise measurement of time over the past 500,000 years. *Earth Planet. Sci. Lett.* **81,** 175–192 (1986/87).
32. Cheng, H. *et al.* The half-lives of uranium-234 and thorium-230. *Chem. Geol.* **169,** 17–33 (2000).
33. Shen, C.-C. *et al.* High-precision and high-resolution carbonate ^{230}Th dating by MC-ICP-MS with SEM protocols. *Geochim. Cosmochim. Acta* **99,** 71–86 (2012).
34. Cheng, H. *et al.* Improvements in ^{230}Th dating, ^{230}Th and ^{234}U half-life values, and U-Th isotopic measurements by multi-collector inductively coupled plasma mass spectrometry. *Earth Planet. Sci. Lett.* **371/372,** 82–91 (2013).
35. Fairchild, I. J. & Baker, A. *Speleothem Science: From Process To Past Environments* p.450 (Wiley–Blackwell, 2012).
36. Dorale, J. A., Edwards, R. L., Ito, E. & González, L. A. Climate and vegetation history of the mid-continent from 75 to 25 ka: a speleothem record from Crevice Cave, Missouri, USA. *Science* **282,** 1871–1874 (1998).
37. Hendy, C. H. The isotopic geochemistry of speleothems—I. The calculation of the effects of different modes of formation on the isotopic composition of speleothems and their applicability as palaeoclimatic indicators. *Geochim. Cosmochim. Acta* **35,** 801–824 (1971).
38. Bowen, G. J. Isoscapes: spatial pattern in isotopic biogeochemistry. *Annu. Rev. Earth Planet. Sci.* **38,** 161–187 (2010).
39. Johnston, V. E., Borsato, A., Spotl, C., Frisia, S. & Miorandi, R. Stable isotopes in caves over altitudinal gradients: fractionation behavior and inferences for speleothem sensitivity to climate change. *Clim. Past* **9,** 99–118 (2013).
40. Vuille, M. & Werner, M. Stable isotopes in precipitation recording South American summer monsoon and ENSO variability: observations and model results. *Clim. Dyn.* **25,** 401–413 (2005).
41. Masson-Delmotte, V. M. *et al.* in *Climate Change 2013: The Physical Science Basis* Ch. 5 (eds Stocker, T. F. *et al.*) 383–464 (Cambridge Univ. Press, 2013).
42. MARGO Project Members. Constraints on the magnitude and patterns of ocean cooling at the Last Glacial Maximum. *Nat. Geosci.* **2,** 127–132 (2009).
43. Marcott, S. A. *et al.* A reconstruction of regional and global temperature for the past 11,300 years. *Science* **339,** 1198–1201 (2013).
44. Thornthwaite, C. W. An approach toward a rational classification of climate. *Geogr. Rev.* **38,** 55–94 (1948).
45. McCabe, G. J. & Markstrom, S. L. A monthly water balance model driven by a graphical user interface. *US Geol. Surv. Open-File Rep.* 2007–1008 (2007).
46. Betts, A. K. & Ridgway, W. Tropical boundary layer equilibrium in the last ice age. *J. Geophys. Res.* **97,** 2529–2534 (1992).
47. Kageyama, M., Harrison, S. P. & Abe-Ouchi, A. The depression of tropical snowlines at the last glacial maximum: what can we learn from climate model experiments? *Quat. Int.* **138-139,** 202–219 (2005).
48. Broecker, W. S. Mountain glaciers: records of atmospheric water vapor content? *Glob. Biogeochem. Cycles* **11,** 589–597 (1997).
49. Rozanski, K., Araguás-Araguás, L. & Gonfiantini, R. in *Climate Change In Continental Isotopic Records* (eds Swart, P. K., Lohmann, K. C., McKenzie, J. & Savin, S.) doi:10.1029/GM078p0001 (Am. Geophys. Union, Washington DC, 1993).
50. Laskar, J. *et al.* A long-term numerical solution for the insolation. *Astron. Astrophys.* **428,** 261–285 (2004).
51. Lüthi, D. *et al.* High-resolution carbon dioxide concentration record 650,000-800,000 years before present. *Nature* **453,** 379–382 (2008).
52. Loulergue, L. *et al.* Orbital and millennial-scale features of atmospheric CH4 over the past 800,000 years. *Nature* **453,** 383–386 (2008).
53. NGRIP Project Members. High-resolution record of Northern Hemisphere climate extending into the last interglacial period. *Nature* **431,** 147–151 (2004).
54. EPICA Community Members. One-to-one coupling of glacial climate variability in Greenland and Antarctica. *Nature* **444,** 195–198 (2006).
55. Veres, D. *et al.* The Antarctic ice core chronology (AICC2012): an optimized multi-parameter and multi-site dating approach for the last 120 thousand years. *Clim. Past* **9,** 1733–1748 (2013).
56. Svensson, A. *et al.* A 60,000 year Greenland stratigraphic ice core chronology. *Clim. Past* **4,** 47–57 (2008).
57. Wang, X. *et al.* Wet periods in northeastern Brazil over the past 210 kyr linked to distant climate anomalies. *Nature* **432,** 740–743 (2004).
58. Anderson, R. F. *et al.* Wind-driven upwelling in the Southern Ocean and the deglacial rise in atmospheric CO_2. *Science* **323,** 1443–1448 (2009).
59. Broecker, W. S. Paleocean circulation during the last deglaciation: a bipolar seesaw? *Paleoceanography* **13,** 119–121 (1998).
60. Buizert, C. *et al.* The WAIS Divide deep ice core WD2014 chronology. Part 1. Methane synchronization (68–31ka BP) and the gas age–ice age difference. *Clim. Past* **11,** 153–173 (2015).
61. Genty, D. *et al.* Precise dating of Dansgaard-Oeschger climate oscillations in western Europe from stalagmite data. *Nature* **421,** 833–837 (2003).
62. Schrag, D. P., Hampt, G. & Murray, D. W. Pore fluid constraints on the temperature and oxygen isotopic composition of the glacial ocean. *Science* **272,** 1930–1932 (1996).
63. Schrag, D. P. *et al.* The oxygen isotopic composition of seawater during the Last Glacial Maximum. *Quat. Sci. Rev.* **21,** 331–342 (2002).
64. Horita, J. & Wesolowski, D. J. Liquid-vapor fractionation of oxygen and hydrogen isotopes of water from the freezing to the critical temperature. *Geochim. Cosmochim. Acta* **58,** 3425–3437 (1994).

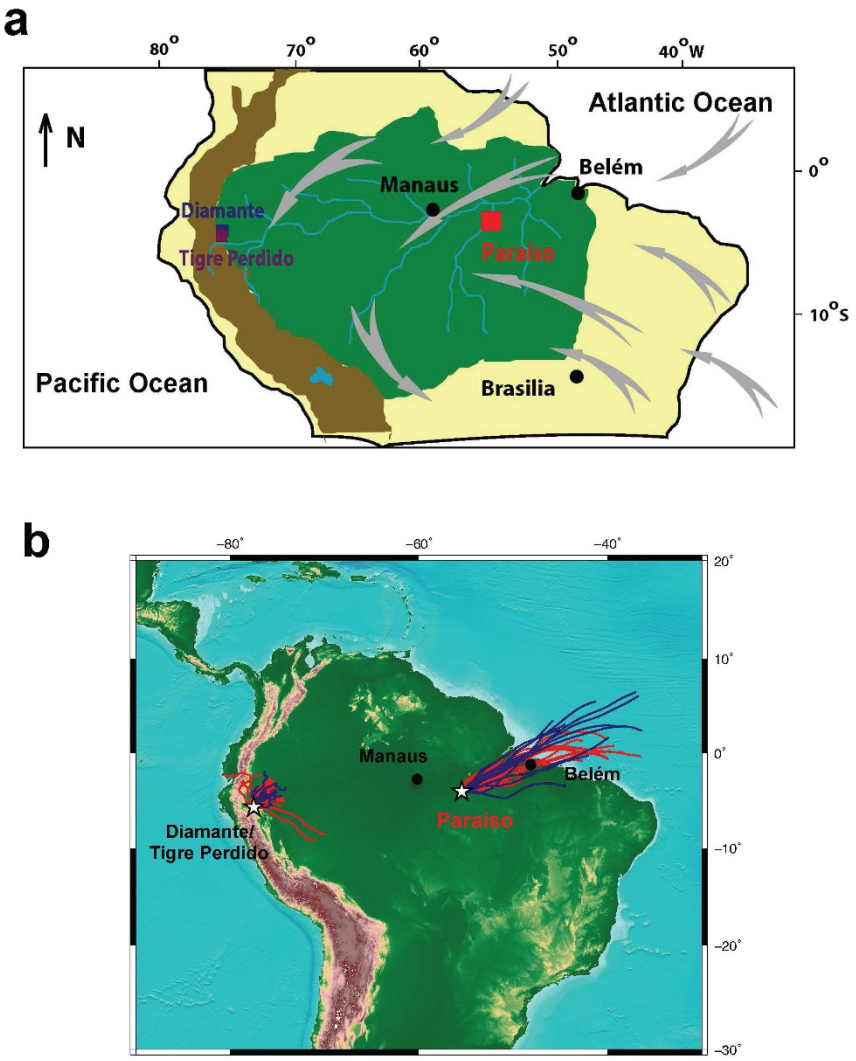

Extended Data Figure 1 | Cave locations and moisture pathways. **a**, The locations of Paraíso Cave in the eastern Amazon (red rectangle), and of Diamante cave[17] (blue rectangle) and Tigre Perdido cave[9] (purple rectangle) in the western Amazon. Paraíso Cave is located between Belém and Manaus, next to the Tapajós River. Also shown are easterlies, which carry moisture to the lowlands from the tropical Atlantic. The Amazon basin and the Andes are shown in green and brown, respectively. **b**, 72-hour back-trajectories of moisture arriving at Paraíso and the western Amazonian cave sites (white stars), during the wet season (in red) and the dry season (in blue), averaged over 1981 to 2010. The background topographical map was created with grid files from the global multi-resolution topography (GMRT) synthesis (http://www.marine-geo.org/tools/GMRTMapTool). Moisture trajectories were derived using the US National Oceanic and Atmospheric Administration (NOAA) Hysplit model (http://ready.arl.noaa.gov/HYSPLIT.php). The moisture at the Paraíso Cave site is predominantly from the tropical Atlantic, whereas precipitation received in the western Amazon has largely endured recycling in the lowlands.

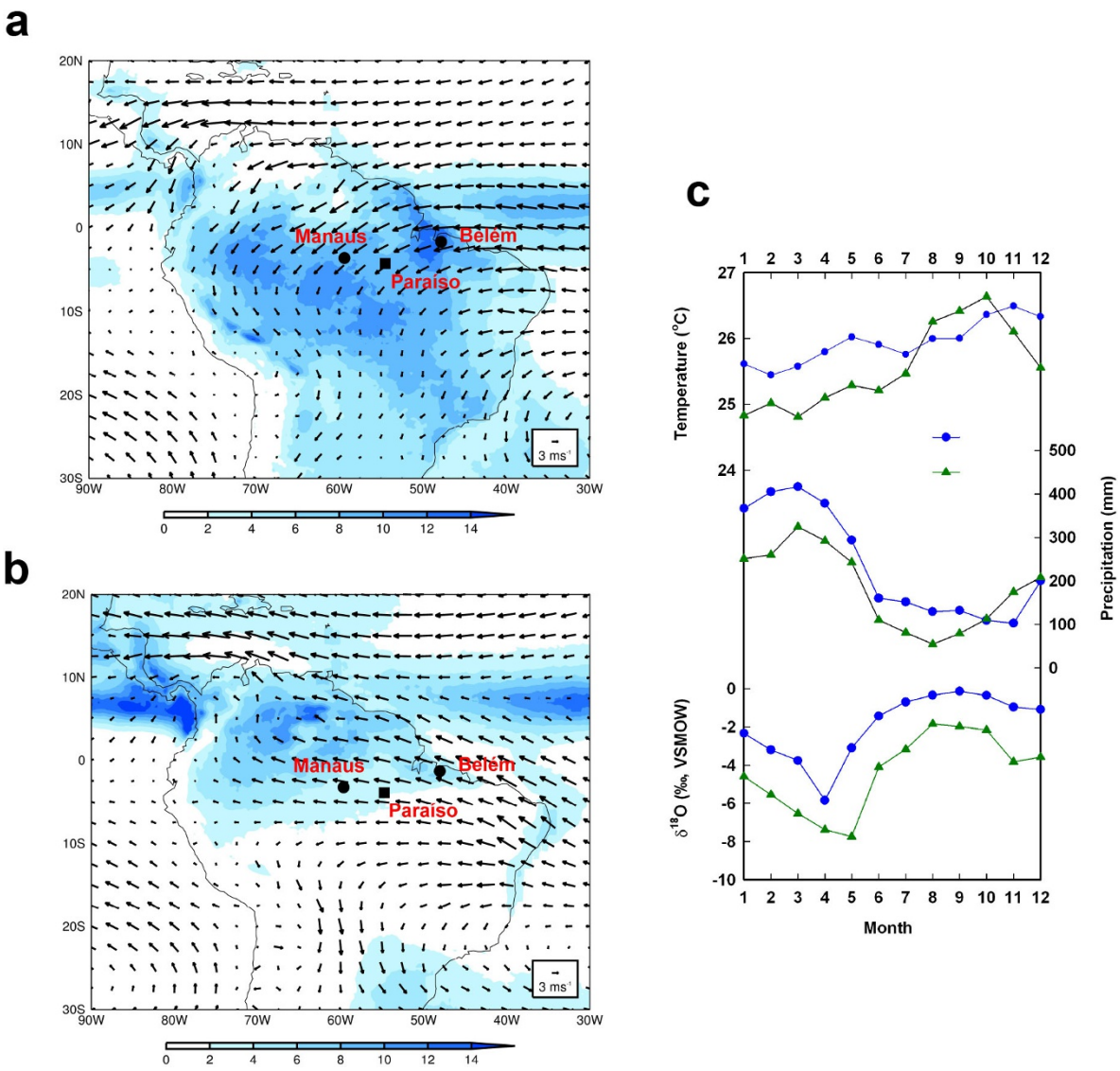

Extended Data Figure 2 | Climatology of tropical South America. **a**, Depiction of horizontal winds over South America at 850 hPa (vectors, in metres per second), based on data from the National Centers for Environmental Prediction (NCEP) Climate Forecast System Reanalysis (CFSR) (1981–2010; http://cfs.ncep.noaa.gov/cfsr/atlas/). Also shown is precipitation (blue shading, in millimetres per day) from the Tropical Rainfall Measuring Mission (TRMM) 3B43 dataset (1998–2010; http://trmm.gsfc.nasa.gov/3b43.html). Winds and precipitation are averaged over December to March. **b**, As in **a**, but for June to September. **c**, Monthly averaged temperature, precipitation and rainfall $\delta^{18}O$ over Belém (blue dots) and Manaus (green triangles). The local climate at Paraíso Cave shares the same characteristics as those of Belém and Manaus. Data are from the International Atomic Energy Agency (IAEA) Global Networks of Isotopes in Precipitation (GNIP) database (http://www-naweb.iaea.org/napc/ih/IHS_resources_gnip.html).

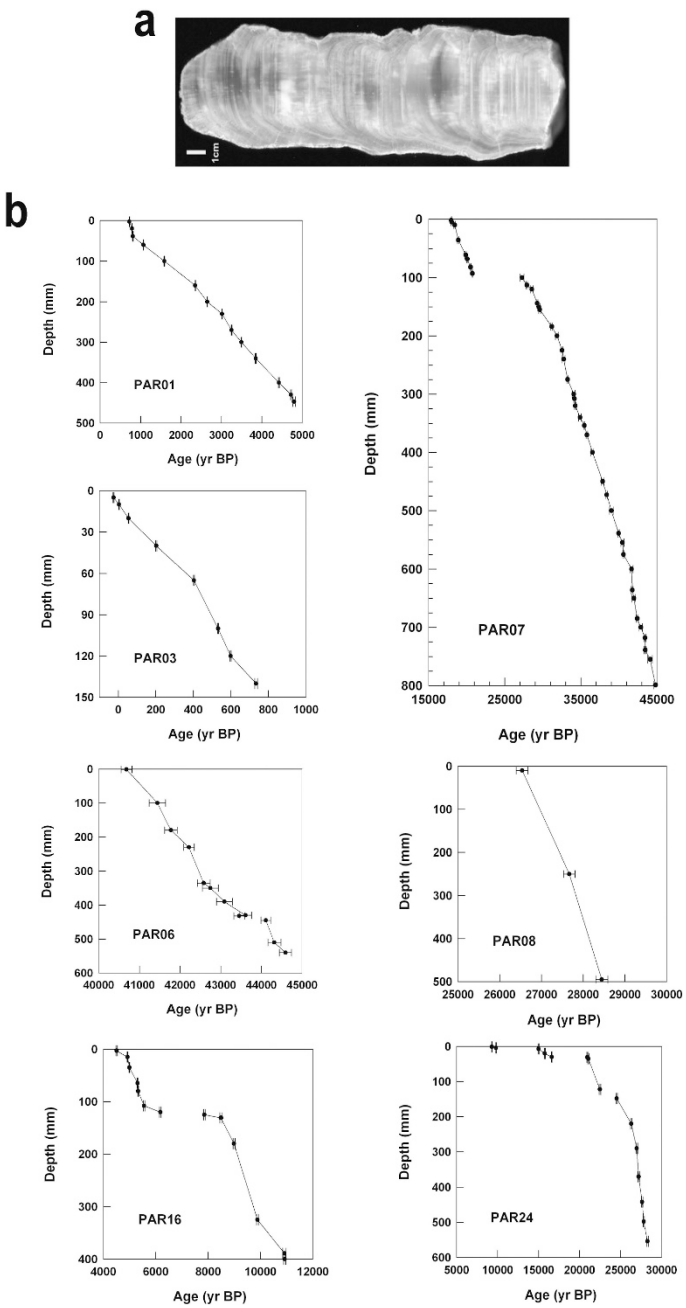

Extended Data Figure 3 | A Paraíso calcite stalagmite, and age models. **a**, Image of a Paraíso sample. The Paraíso calcite stalagmites typically have a high uranium concentration (up to 40 p.p.m.) but a low thorium concentration (<1 parts per billion, p.p.b.), almost ideal for uranium/thorium-based age determination. **b**, Age models for samples PAR01, PAR03, PAR06, PAR07, PAR08, PAR16 and PAR24. The chronology of the samples is established by linear interpolation between successive uranium/thorium dates. Dates are shown in black dots. Age uncertainties (2σ) are also included (most of the error bars are smaller than the symbols).

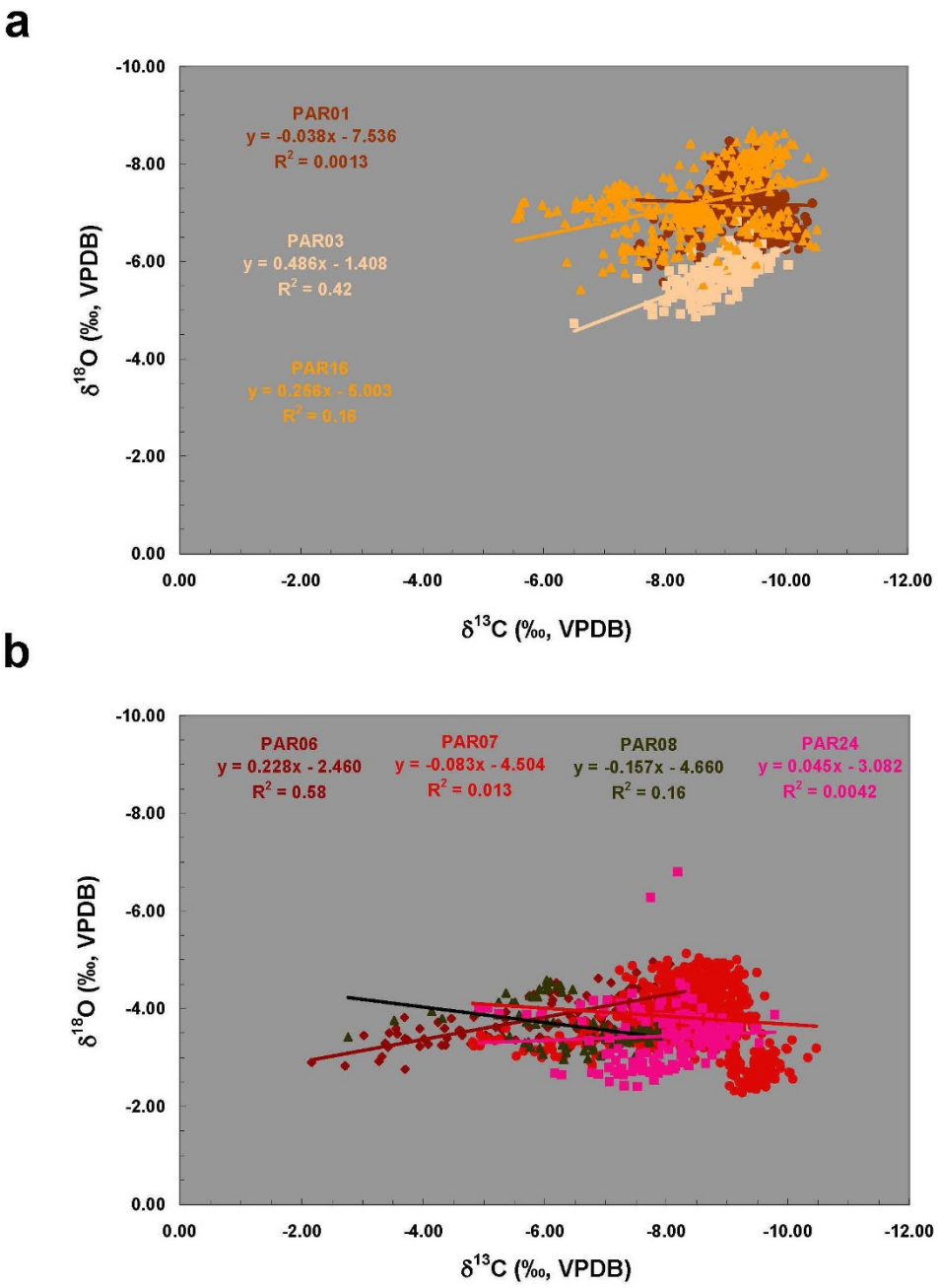

Extended Data Figure 4 | Scatterplots of oxygen and carbon isotope ratios for the Paraíso stalagmites. a, Relationship between the $\delta^{18}O$ and $\delta^{13}C$ data for Holocene Paraíso stalagmites. **b**, As in **a**, but for glacial Paraíso samples.

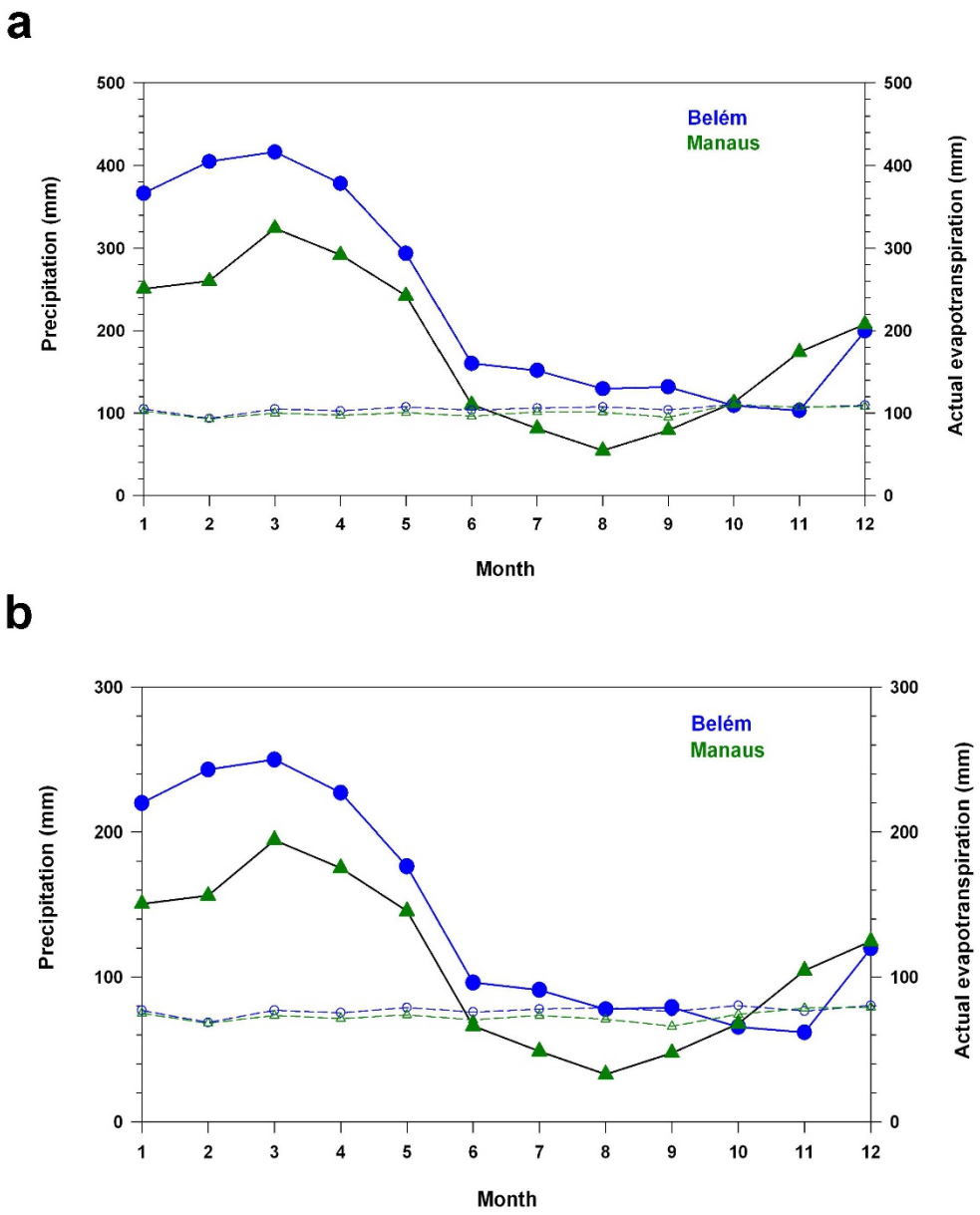

Extended Data Figure 5 | Estimation of monthly water balance in the region. a, Monthly averaged precipitation (solid dots and triangles) and actual evapotranspiration (AET, open dots and triangles) over Belém and Manaus. We used the water-balance model[44] as implemented in the US Geological Survey (USGS) Thornthwaite model[45] to calculate monthly AET. **b**, As in **a**, but for LGM conditions. We assume that the cave temperature was ~21 °C during the LGM. Rainfall in the region was ~60% of today's in each month, as calculated in Extended Data Table 1. The LGM and present-day patterns are essentially the same.

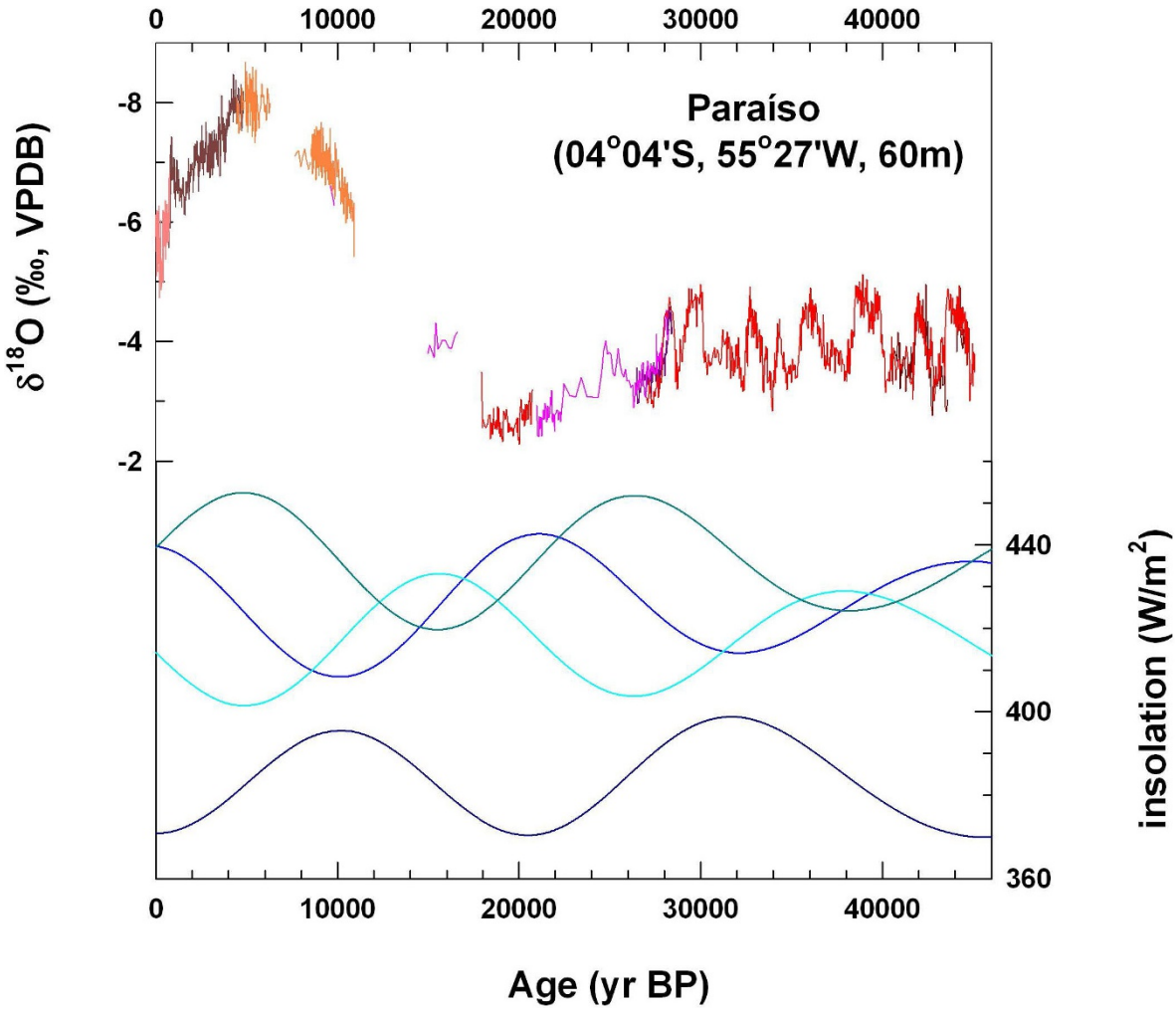

Extended Data Figure 6 | Comparisons of the Paraíso record with local insolation curves. The cave $\delta^{18}O$ record spans about 46,000 years, long enough to cover two precessional cycles. However, no obvious correlation can be observed between the cave record with local insolation in the months of January (blue), April (cyan), July (dark blue) and October (dark cyan). Insolation data are from ref. 50.

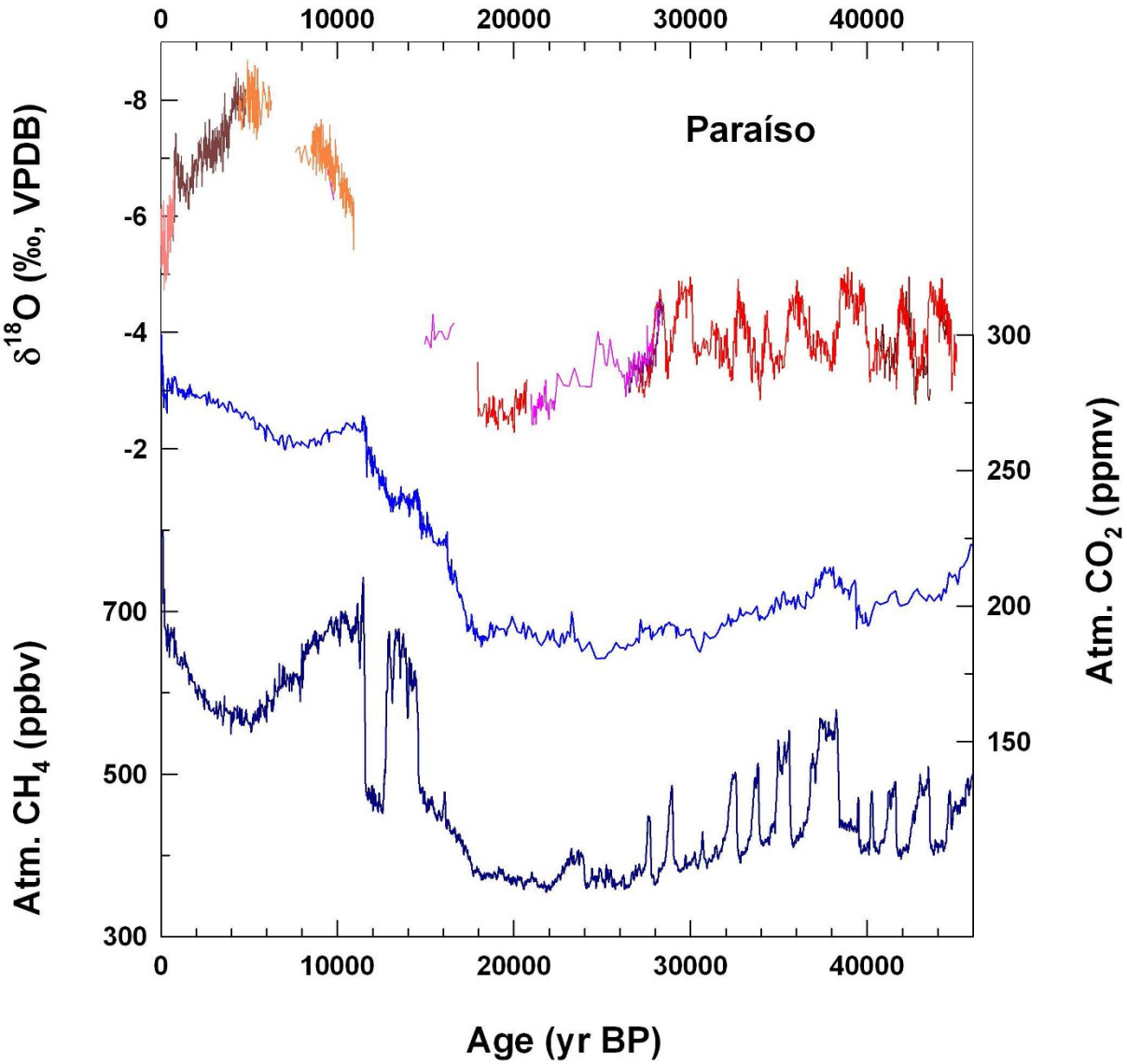

Extended Data Figure 7 | Comparisons of the Paraíso $\delta^{18}O$ record with atmospheric concentrations of greenhouse gases. Changes in atmospheric CO_2 (blue) and CH_4 (dark blue) concentrations are recorded in Antarctic ice cores[51,52].

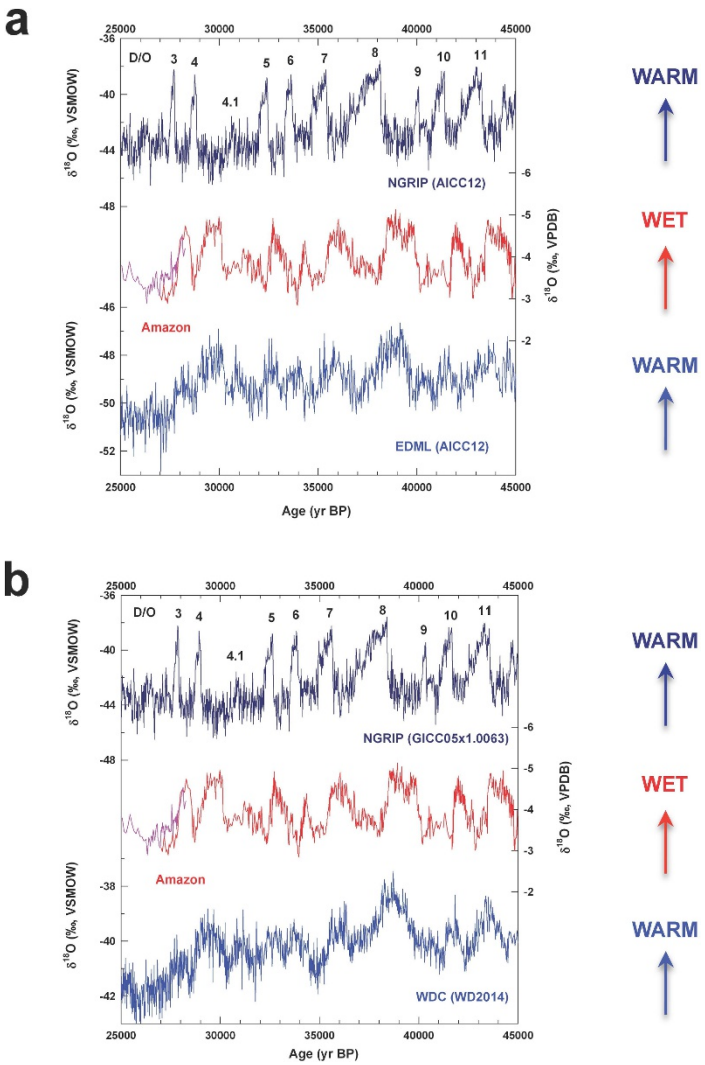

Extended Data Figure 8 | Comparisons of the Paraíso cave record and ice-core records. a, The Paraíso $\delta^{18}O$ record is compared with ice-core records from Greenland[53] (dark blue; North Greenland Ice Core Project (NGRIP)) and from Antarctica[54] (blue; EPICA Dronning Maud Land (EDML) Ice Core) during the time interval from 25 kyr BP to 45 kyr BP. The NGRIP ice-core data are plotted in the Antarctic ice-core chronology 2012 (AICC12) timescale[55], which is identical to the annual-layer-counted Greenland ice-core chronology 2005 (GICC05) timescale[56] for the studied time interval. The EDML ice-core data are plotted in the AICC12 age scale[55]. D/O events are marked on the NGRIP record. The strong correlations between the Paraíso record and the ice-core records confirm the existence of rapid air–sea interactions between the high latitudes and the tropics on millennial timescales[57,58], probably through the so-called bipolar seesaw mechanism[59]. **b**, As in **a**, but the Paraíso record is compared with ice-core records from Greenland[53] (dark blue; NGRIP) and from Antarctica[25] (blue; West Antarctic Ice Sheet Divide Ice Core (WDC)). The NGRIP and WDC data are plotted in the West Antarctic Ice Sheet Divide (WD) 2014 timescale[25]. The slightly enhanced correlations between the Paraíso record and the ice-core records, albeit visually, support the chronological method adopted in ref. 60. VSMOW, Vienna standard mean ocean water.

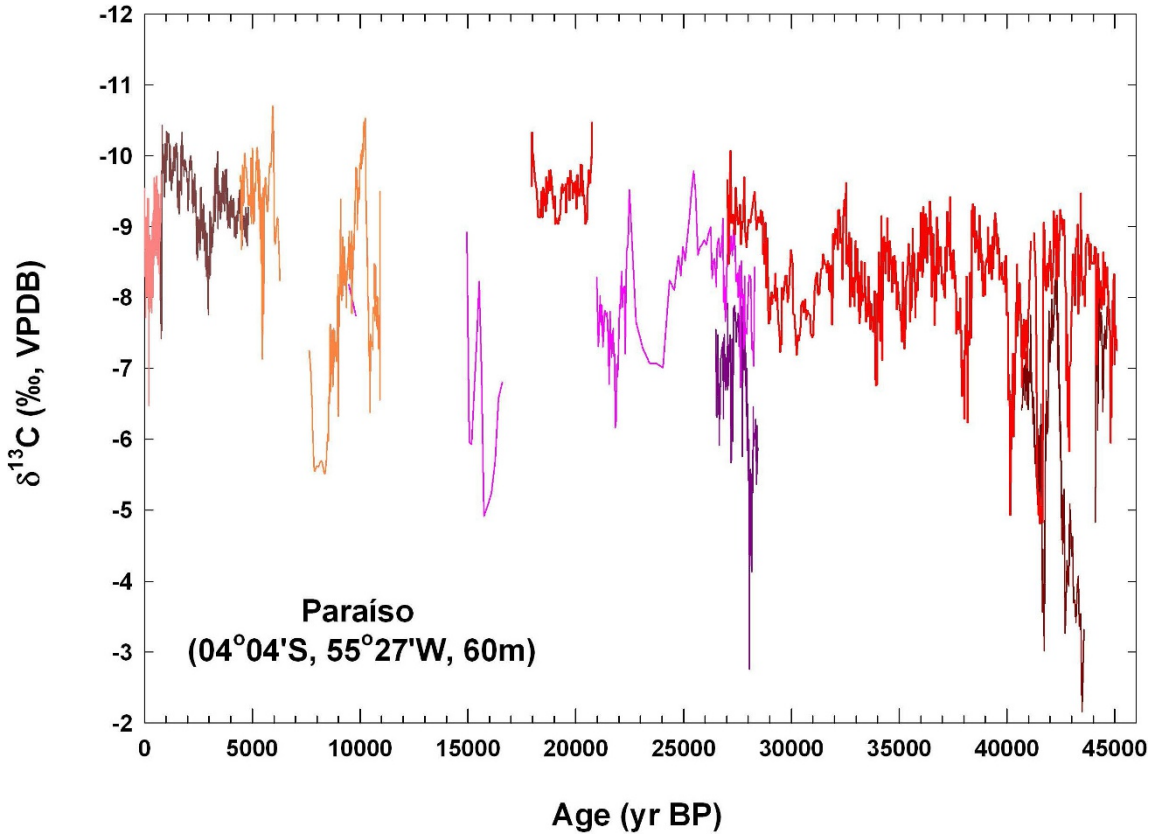

Extended Data Figure 9 | Paraíso $\delta^{13}C$ record. Contrary to the stalagmite $\delta^{18}O$ record, the Paraíso $\delta^{13}C$ record does not show an obvious shift from the last glacial period to the Holocene. In fact, the $\delta^{13}C$ value reaches as low as about −10‰ during the LGM, similar to the observed minimum value in the Holocene. This suggests that the type of vegetation in the region has not undergone dramatic changes, remaining dominated by C3 plants[37,61]. The rainforest in the eastern Amazon might have become an open forest when the precipitation decreased substantially during the LGM. However, it was not replaced by savanna or grassland—that is, it has not become dominated by C4 plants. The $\delta^{13}C$ spikes were probably caused by individual air–water–rock interactions during calcite precipitation.

Extended Data Table 1 | Calculations of water vapour loss over the eastern Amazon

a

Time Interval	Cave temp. (°C)	$\delta^{18}O_c$ (‰, VPDB)	$\delta^{18}O_p$ (‰, VSMOW)	$\delta^{18}O_{sw}$ (‰, VSMOW)	Water vapor remained in air masses (%)	Amount lost wrt. modern value (%)
Modern	26	-5.7 (n = 145, 1σ = 0.4)	-4.1	0.0	64	100
Mid-Holocene	26.5	-8.0 (n = 80, 1σ = 0.3)	-6.3	0.0	50	142
LGM	21	-2.7 (n = 101, 1σ = 0.2)	-2.1	1.0	72	58

b

Time Interval	Cave temp. (°C)	$\delta^{18}O_c$ (‰, VPDB)	$\delta^{18}O_p$ (‰, VSMOW)	$\delta^{18}O_{sw}$ (‰, VSMOW)	Water vapor remained in air masses (%)	Amount lost wrt. modern value (%)
Modern	26	-5.7 (n = 145, 1σ = 0.4)	-4.1	0.0	64	100
Mid-Holocene	26	-8.0 (n = 80, 1σ = 0.3)	-6.4	0.0	50	139
LGM	20	-2.7 (n = 101, 1σ = 0.2)	-2.3	1.0	71	57
LGM	22	-2.7 (n = 101, 1σ = 0.2)	-1.9	1.0	74	58

Top, temperature was assigned to be 5 °C lower in the LGM, and 0.5 °C warmer during the mid-Holocene, relative to modern values. $\delta^{18}O_c$ is calcite $\delta^{18}O$ value, read from the Paraíso speleothem record. $\delta^{18}O_p$ is the local precipitation $\delta^{18}O$ value, calculated using an isotopic fractionation factor between calcite and water, α, derived from the following equation: $1{,}000 \times \ln\alpha$ (calcite–H_2O) $= 17.66 \times (10^3 \times T^{-1}) - 30.16$, where T is the temperature (in kelvin)[39]. $\delta^{18}O_{sw}$ is sea water $\delta^{18}O$, assigned to be 0‰ for today and the mid-Holocene, and 1‰ in the LGM[62,63]. The fraction of water vapour remaining was calculated using the Rayleigh fractionation equation: $(1{,}000 + \delta^{18}O_p)/(1{,}000 + \delta^{18}O_{sw}) = f^{(\alpha - 1)}$, where f is the fraction of the original water vapour remaining in air masses, and α is the isotopic fractionation factor between water liquid and vapour phases[64]. The percentage of water vapour removed from air masses after reaching the cave site is about 36%, 50% and 28% for the present (modern) day, the mid-Holocene, and the LGM, respectively. Given a relative humidity of 100%, the absolute humidity (AH, in g m^{-3}) can be calculated from the equation: $AH = (C \times e_s)/T$, where C is a constant with a value of 2,165 g K J^{-1}; e_s is the saturation vapour pressure (in kPa); and T is the temperature (in kelvin). We obtained an absolute humidity of ~24.3 g m^{-3}, 25.0 g m^{-3} and 18.3 g m^{-3} for the present day, the mid-Holocene and the LGM, respectively. So, the absolute humidity in this equatorial region was about 103% and 75% of today's value during the mid-Holocene and the LGM, respectively. The amount of moisture removed from air masses is then calculated relative to the modern value (set as a reference point at 100%).
Bottom, as for top, except that, to test the sensitivity of water vapour loss to temperature, we applied different temperatures for the mid-Holocene (for example, the same as the present-day temperature) and LGM (for example, 4 °C or 6 °C lower than the present temperature).